PERGAMON

International Journal of Solids and Structures 37 (2000) 599–625

INTERNATIONAL JOURNAL OF SOLIDS and STRUCTURES

www.elsevier.com/locate/ijsolstr

On some aspects of pin-loaded laminates

Chien-Chang Lin*, Chuen-Horng Lin [1], James T.S. Wang [2]

Department of Applied Mathematics, National Chung-Hsing University, College of Science, Taichung 40227, Taiwan

Received 7 April 1998; in revised form 28 December 1998

Abstract

Some aspects of pin loaded laminates, including basic kinematics related to the contact angle and moving boundary, validity and applicability of cosine distribution of contact stress, effects of stiffness ratios as well as clearance and friction are presented. Numerical results on the basis of a previously developed direct boundary element procedure, with a refined and improved computational algorithm with additional capabilities are given and used for discussing various aspects of pin-loaded orthotropic laminates. Empirical formulas based on generated computer results are suggested.

Keywords: Contact angle; Cosine distribution; Clearance; Friction; Contact stresses; Direct boundary element; Formulae

1. Introduction

The distribution of contact stresses along the edge of a pin-loaded hole in a plate has been an important issue. Due to the complexity of the problem which involves moving boundary conditions as the contact region between the pin and hole edge and depends on the magnitude of the load and other geometrical and material parameters, many researchers have studied the problem by using various numerical methods. While numerous studies have provided a good insight to the physical phenomena and general understanding of the problem, the present state of the art still cannot be easily used by designers. As an engineering approach, a simple cosine distribution of the radial contact stress is often used. On the basis of such an assumption, Jong (1977), and Zhang and Ueng (1984) used complex stress functions, and Mangalgiri et al. (1987) used an inverse technique to study stresses in an orthotropic plate of

* Corresponding author. Fax: +00886-4287-3028.
E-mail address: cclin@amath.nchu.edu.tw (C.C. Lin)
[1] Current address: National Taichung Institute of Commerce of Taiwan.
[2] Visiting from Georgia Institute of Technology.

0020-7683/00/$ - see front matter
PII: S0020-7683(99)00025-6

Nomenclature

E_{11}	Young's modulus in the longitudinal direction.
E_{22}	Young's modulus in the transverse direction.
G_{12}	shear modulus.
ν_{12}	Poisson's ratio.
t	surface traction.
u	displacement.
D	hole diameter.
R	hole radius.
a	pin radius.
h	thickness of the plate.
W	width of the plate.
L	length of the plate.
d_1	plate edge distance from the hole center and the plate edge.
c_{ij}	stiffness constants.
F_{ij}	Green's function for traction.
H_{ij}	Green's function for displacement.
μ	coefficient of static friction.
e	clearance between the hole and the pin.
δ	pin displacement.
ϕ	polar angle with respect to the hole center.
ψ	polar angle with respect to the pin center.
α	one half of the total angle of contact.
β	one half of the total contact angle of no-slip regions.
u_x, u_y	displacement components of the hole-edge.
t_x, t_y	traction components of the hole-edge.
u_r	radial displacement of the hole-edge.
σ_r, σ_ϕ, $\tau_{\mathrm{r}\phi}$	stresses in polar coordinates.
σ_b	average bearing stress.
σ_0	normal stress on the hole boundary at $\phi = 0$.
σ_p	peak normal stress on the hole boundary.
ϕ_p	location of the peak normal stress.
σ_β	normal contact stress at $\phi = \beta$.
$\varepsilon_\phi^\mathrm{p}$	circumferential strain of the hole along the hole edge.
S	average normal stress.

infinite size under a load from a perfectly fitted frictionless pin. All of these analytical solutions considered the plate to be of infinite size. Wong and Matthews (1981), Chang et al. (1983), Chang (1986), Chang and Scott (1984a, 1984b), and Tsujimoto and Wilson (1986) used the finite element method for finite sized plates. Mahajerin and Sikarskin (1986), and Lin and Lin (1993) used the boundary element method. Also, Eshwar (1978) and Ghosh and Rao (1981) used complex stress functions for infinite sized plates with a perfectly fitted pin. None of these studies addressed the pin-hole interaction as the pressure at the contact surface is pre-assumed to vary as a cosine function.

There are studies accounting for the interaction between the pin and the hole. Hyer and Klang (1985)

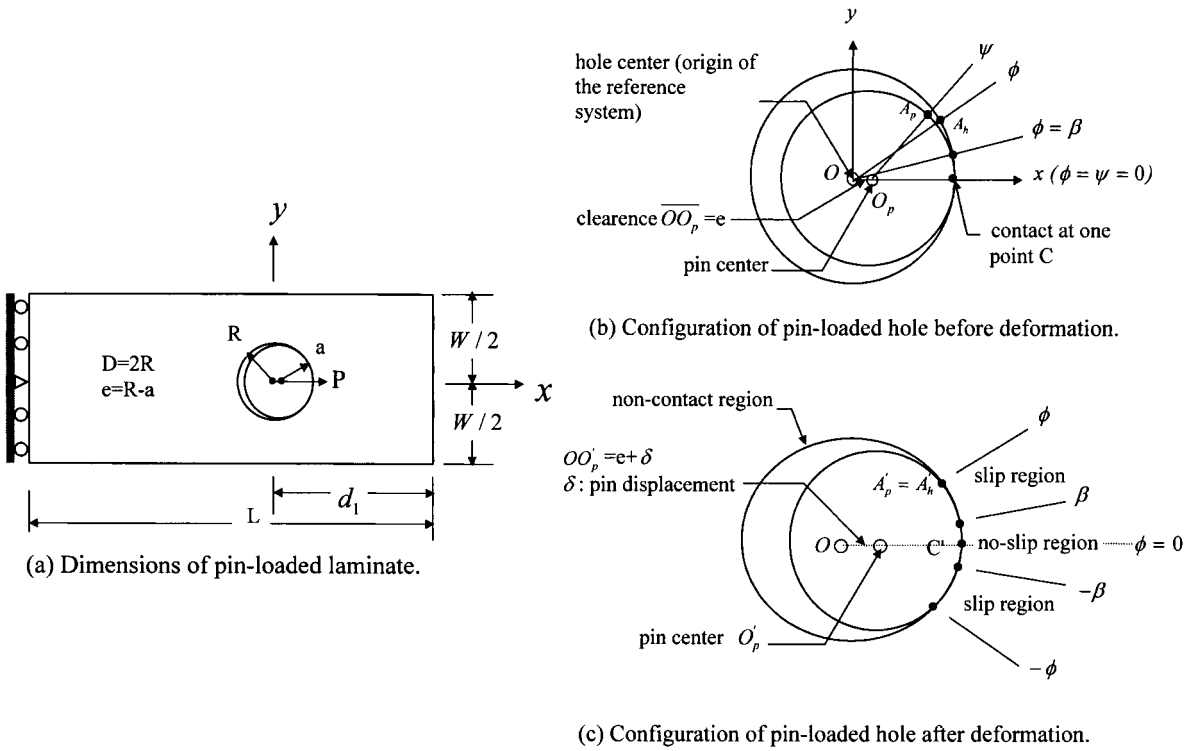

Fig. 1. Geometry and coordinate system for pin-loaded laminate.

and Hyer et al. (1987) used a complex Fourier series in conjunction with boundary collocations. Agarwal (1980), Rahman (1984), Naik and Crews (1986), Yogeswaren and Reddy (1988), Rahman and Rowlands (1993), Eriksson et al. (1995), Blackie and Chutima (1996), and Camanho and Mattews (1997) used finite element methods. Experimental studies were made by Waszczak and Cruse (1971), Quinn and Matthews (1977), Pyner and Matthews (1979), Tsai and Morton (1990), and Cooper and Turvey (1995).

Lin and Lin (1999) have established a direct boundary element procedure to study the contact stresses around a pin loaded hole in composite laminates. Results compare well with earlier works such as those given by Hyer and Klang (1985) and Hyer et al. (1987). While the established boundary element method is effective, the procedure used in Lin and Lin (1999) has been further improved for its computational efficiency with added capability for computing deformation and stresses in generally orthotropic laminates of finite size. Data can be generated to establish empirical formulae to help simplify the analysis procedure for designers.

2. The model, basic relations and conditions

Generally orthotropic laminates of finite size subjected to a load, P, in the longitudinal x direction from a rigid pin allowing a clearance and accounting for friction between the pin and the hole edge are considered for the modeling of the problem. The geometry, coordinate systems and some symbols are shown in Fig. 1. The pin-loaded plate is finite and the initial origins of coordinate systems are placed at

the hole center, O, of the plate. The clearance, e, is the difference in radii of the hole and the pin. The coefficient of static friction, μ, is used for identifying whether parts of the contact region slip or not. ϕ and ψ are polar angles of coordinate fixed on the plate and pin, respectively. The angle 2α represents the total contact region, whereas the angle 2β identifies the no-slip region.

2.1. Angle of contact 2α

If there is no clearance, the pin and the hole edge are in contact everywhere with the contact angle of $2\alpha = 360^\circ$ or $\alpha = 180^\circ$ before the load is applied. Once the deformation of the hole occurs, one part of the hole separates from the pin while the rest remains in contact. The last two points on the pin which can be in contact with the hole are at $\psi = \pm 90^\circ$. Hence, if the edge of the hole is inextensible in the circumferential direction, the contact arc length of the hole edge being $2\alpha R$ must be equal to one half of the pin surface of $a\pi$. The angle α, identifying the contact region, becomes 90° for $a = R$. However, since the edge of the hole is extensible in the circumferential direction, α decreases from 90° as the load increases or as the pin is moved forward. So, as soon as there is a load or the pin has a slight movement, α drops momentarily to about 90° and continues to reduce as the load increases.

On the other hand, if there is a clearance, the pin contacts the hole at the point corresponding to $\phi = \psi = 0^\circ$ when no load is transmitted, or the pin is just moved by the amount of the clearance, e. The contact angle α gradually increases as the load increases.

Consequently, the angle α identifying the extent of the contact region decreases for no clearance case, while α increases for $e > 0$ as the load increases. Although, there is no limiting value for α as the hole edge is extensional in the circumferential direction, the upper bound limit corresponding to an inextensible hole is

$$\alpha_{\max} = \frac{a\pi}{2R}. \tag{1}$$

2.2. Kinematics of moving boundary

The matching points of contact on the hole edge and pin surface change as the load P changes. Such a contact interface may be referred to as a moving boundary. After the plate is deformed due to the movement of the pin as shown in Fig. 1, the point of contact C moves to C' and a point A_{h} on the hole moves to A'_{h}, which matches A'_{p} displaced from the point A_{p} of the pin. As a result, the circumferential length $C'A'_{\mathrm{h}}$ of the hole edge must be equal to the length $C'A'_{\mathrm{p}}$ as well as CA_{p}. Assuming a rigid pin, we arrive at

$$a\psi = \int_0^{\phi} R\left(1 + \varepsilon_{\phi}^{\mathrm{h}}\right)\mathrm{d}\phi = R\phi + R\int_0^{\phi} R\varepsilon_{\phi}^{\mathrm{h}}\,\mathrm{d}\phi, \tag{2}$$

in which the superscripts 'p' and 'h' denote the pin and the hole, respectively; $\varepsilon_{\phi}^{\mathrm{h}}$ is the circumferential strain along the hole boundary.

2.3. Contact interface

The following compatibility conditions in displacement between the pin and the hole on the no-slip contact surface ($-\beta < \phi < \beta$) must be satisfied:

$$R\cos\phi + u_x = a\cos\psi + (e + \delta)\ (-\beta < \phi < \beta) \tag{3a}$$

$$R\sin\phi + u_y = a\sin\psi \ (-\beta < \phi < \beta) \tag{3b}$$

at $r = R$ where r is the radial coordinate with respect to the center of the hole, u_x and u_y are displacements of the hole-edge in the x- and y-directions, respectively, and δ is the longitudinal movement of the pin beyond the first contact. In the slip region ($\beta \le \phi < \alpha$) and ($-\alpha < \phi \le -\beta$), the following compatibility of the displacement in the radial direction of the pin and hole edge

$$u_r = u_x\cos\phi + u_y\sin\phi = [e + \delta + a\cos\psi]\cos\phi + a\sin\psi\sin\phi - R \ (-\alpha < \phi \le -\beta \text{ and } \beta \le \phi < \alpha) \tag{4a}$$

and the force condition

$$|\tau_{r\phi}| = \mu|\sigma_r| \ (-\alpha < \phi \le -\beta \text{ and } \beta \le \phi < \alpha) \tag{4b}$$

for $r = R$ are to be satisfied, where u_r is the radial displacement of the hole-edge and μ is the coefficient of static friction between the pin and hole edge. In the non-contact region along the hole-edge ($\alpha \le \phi \le 2\pi - \alpha$), the radial and shear stresses σ_r and $\tau_{r\phi}$ are zero.

To accommodate the computational algorithm, Eq. (4b) is based on the relationships

$$\sigma_r = t_x\cos\phi + t_y\sin\phi, \quad \tau_{r\phi} = -t_x\sin\phi + t_y\cos\phi, \tag{5a}$$

when $\sigma_r < 0$ is rewritten as follows:

$$t_y = \frac{\sin\phi + \mu\cos\phi}{\cos\phi - \mu\sin\phi}t_x \ (-\alpha < \phi \le -\beta \text{ and } \beta \le \phi < \alpha), \tag{5b}$$

where negative σ_r denotes compressive stress.

The conditions required by eqns Eqs. (3a), (3b) and (4a) involve the angle ψ which locates the matching point on the pin to that on the hole defined by ϕ. The exact relation of ψ to ϕ is given in Eq. (2), which involves the circumferential strain along the contact region of the hole edge. For this relationship to be satisfied on the moving boundary would require an iterative procedure which makes the analysis extremely difficult, if not impossible. Hyer and Klang (1985) and Hyer et al. (1987) simply take $\psi = \phi$ without specific explanation, while Lin and Lin (1999) proposed $a\psi = R\phi$ based on kinematic reasoning. Inasmuch as the contribution of ε_ϕ^h is believed to be small, the use of the $a\psi = R\phi$ relation including the clearance effect would be adequate. An alternative possibility for an improved approximation is to assign an estimated average circumferential strain for the contact region. In the present study, all numerical results are computed by neglecting the circumferential strain effect but including the clearance effect. According to the limited results obtained in the study, the maximum average circumferential strain is in the order of about 6 percent.

3. Analysis

The direct boundary element method derived from the work of Banerjee and Butterfield (1981) and used in Lin and Lin (1999) is followed. If no body force exists, as is considered in the present study, the basic resulting equation for determining the displacement is

$$\kappa u_j(\xi) = \int_S [t_i(x)H_{ij}(x,\xi) - F_{ij}(x,\xi)u_i(x)]\mathrm{d}s(x), \tag{6}$$

in which the value of κ equals 1 when point ξ is inside of s, 1/2 when ξ lies on s, and zero when ξ is outside of s; x locates an interior point and ξ for a boundary point; F_{ij} and H_{ij} are Green's functions for traction and displacements, respectively, at a point x in the i direction due to a unit force applied at point ξ in the j direction, and u_i and t_i are the displacement and traction, respectively. Other details and discussions on the use of integral formulations for the direct boundary element method and the fundamental solution given in Rizzo and Shippy (1970) can be found in Lin and Lin (1999).

3.1. Discretization of the boundary

A detailed descriptions on discretization can be found in Lin (1998); a brief discussion is presented here. The entire boundary is divided into M quadratic elements which consist of M_{c_1}, M_{c_2} and M_{nc} elements for slip contact regions, no-slip contact regions, and the remaining non-contact hole edge and the exterior boundary of the plate, respectively. Each element has three nodes with two end nodes joined to adjacent elements. Each node of an element has two displacement and two traction components. Due to geometric compatibility, only two displacement components for each set of the common end nodes joined to adjacent elements are used, while two traction components are required to describe the force state at each end node. From Eq. (6), we can relate the displacement vector of a nodal point p in terms of tractions or displacements at all $(2M)$ nodal points on the entire boundary as

$$\frac{1}{2}\{u^p\} = \sum_{q=1}^{M}\left[\int_{S_q} H^{pq} N \,\mathrm{d}S\right]\{t^q\} - \sum_{q=1}^{M}\left[\int_{S_q} F^{pq} N \,\mathrm{d}S\right]\{u^q\} \ (p = 1,2,\ldots,2M), \tag{7}$$

where N is the shape function. Eq. (7) can be represented by simple matrix equation, as follows:

$$[F]\{u\} = [H]\{t\}, \tag{8}$$

in which $\{u^p\}$ has been merged into $\{u\}$, and $[F]$ and $[H]$ are $4M \times 4M$ and $4M \times 6M$ matrices, respectively; $\{u\}$ and $\{t\}$ have dimensions of $4M \times 1$ and $6M \times 1$, respectively.

In the slip region along the contact surface of the hole boundary, one needs to specify one displacement component given in Eq. (4a) for compatibility, and one traction component given in Eq. (5b) for the force condition at each of the $2M_{c_1}$ nodal points. Thus, the number of equations involved in Eq. (8) can be reduced and written in the following form:

$$[\bar{F}]\{u\} + [\bar{F}_B] = [\bar{H}]\{t\}, \tag{9}$$

in which $[\bar{F}]$ and $[\bar{H}]$ are reduced to $4M \times (4M_{\mathrm{nc}} + 2M_{c_1} + 4M_{c_2})$ and $4M \times (6M_{\mathrm{nc}} + 2M_{c_1} + 4M_{c_2})$ matrices, respectively, and $[F_B]$ is a $4M \times 1$ matrix; $\{u\}$ and $\{t\}$ are reduced to $(4M_{\mathrm{nc}} + 2M_{c_1} + 4M_{c_2}) \times 1$ and $(6M_{\mathrm{nc}} + 2M_{c_1} + 4M_{c_2}) \times 1$, respectively. Note that subscripts nc denote the part of the boundary other than the contact region of the hole edge. The matrices $[F]$, $[F_B]$ and $[H]$ in Eq. (9) are related to $[F]$ and $[H]$ in Eq. (8) through the use of Eqs. (4a) and (5b) as follows:

$$\left[\bar{F}^{M_{c_1}}_{i,j-1}\right] = \left[F^{M_{c_1}}_{i,j-1}\right] - \left[F^{M_{c_1}}_{i,j}\right]\cot\phi,$$

$$\left[\bar{F}^{M_{c_1}}_{B_i}\right] = \left[F^{M_{c_1}}_{B_i}\right] + \left[\left(\delta + e + a\cos\left(\frac{R}{a}\phi\right)\right)\cos\phi + a\sin\left(\frac{R}{a}\phi\right)\sin\phi - R\right]\frac{\left[\bar{F}^{M_{c_1}}_{i,j}\right]}{\sin\phi},$$

$$\left[\bar{F}_{i,j}^{M_{c_1}}\right] = 0 \begin{cases} i = 1,2,\ldots,4M \\ j = 2,4,\ldots,4M_{c_1} \quad (j = \text{even}) \end{cases} \tag{10}$$

and

$$\left[\bar{H}_{i,j-1}^{M_{c_1}}\right] = \left[H_{i,j-1}^{M_{c_1}}\right] + \left[H_{i,j}^{M_{c_1}}\right]\left(\frac{\sin\phi + \mu\cos\phi}{\cos\phi - \mu\sin\phi}\right),$$

$$\left[\bar{H}_{i,j}^{M_{c_1}}\right] = 0 \begin{cases} i = 1,2,\ldots,4M \\ j = 2,4,\ldots,6M_{c_1} \quad (j = \text{even}) \end{cases}. \tag{11}$$

Using the $6M_{nc} + 4M_{c_2}$ tractions or displacements given from the boundary conditions at all $2M_{nc}$ nodes and all $2M_{c_2}$ nodal points, Eq. (9) can be rewritten in the following form:

$$[A]\{X\} = [B]\{Y\}, \tag{12}$$

where $[A]$ is a $4M \times 4M$ matrix and $\{X\}$ contains the $4M \times 1$ unknown traction and displacement components, $[B]$ is a $4M \times (6M_{\text{nc}} + 4M_{c_2})$ matrix, and $\{Y\}$ contains the given $(6M_{\text{nc}} + 4M_{c_2})$ boundary quantities. It may be noted that if the M_c number of corner points on the 'nc' part of the boundary can be identified, then $6M_{nc}$ can be reduced to $(4M_{nc} + 2M_c)$. Clearly, if the entire boundary is perfectly smooth, $6M_{nc}$ can further be reduced to $4M_{nc}$.

3.2. Displacements and stresses in the plate

Most of the previous studies, including the authors' earlier work (Lin and Lin, 1999), were focused on the investigation of contact stresses between the pin and the hole edge. The work presented in Lin and Lin (1999) has been expanded to include the capability of determining displacements and stresses in the plate to examine deformation and determine the state of stress for eventual design applications. To solve the boundary value problem in plane elasticity using the fundamental solution, the displacement and traction at each boundary element are given. As a result, the displacement at any point, $\bar{p}$, can be determined from the known values of the displacements and tractions from the boundary points as follows:

$$\left[u_j^{\bar{p}}\right] = \sum_{q=1}^{M}\left[\int_S H_{ij}^q N \,\mathrm{d}S\right]\left\{t_i^q\right\} - \sum_{q=1}^{M}\left[\int_S F_{ij}^q N \,\mathrm{d}S\right]\left\{u_i^q\right\} \ (i,j = 1,2), \tag{13}$$

from which the strain components, ε_x, ε_y and γ_{xy}, can be determined subsequently. The stresses at a point can then be determined from the following stress–strain relation:

$$\begin{Bmatrix} \sigma_x \\ \sigma_y \\ \sigma_{xy} \end{Bmatrix} = \begin{bmatrix} c_{11} & c_{12} & 0 \\ c_{12} & c_{22} & 0 \\ 0 & 0 c_{66} & \end{bmatrix} \begin{Bmatrix} \varepsilon_x \\ \varepsilon_y \\ \gamma_{xy} \end{Bmatrix}, \tag{14}$$

in which the stiffness constants, c_{ij}, and the stresses, σ_{ij}, are taken as mean values through the thickness of the laminate. The stress components may be expressed as follows:

$$\left[\sigma_{ij}^{\bar{p}}\right] = \sum_{q=1}^{M}\left[\int_S D_{ijk}^q N \,\mathrm{d}S\right]\left\{t_k^q\right\} - \sum_{q=1}^{M}\left[\int_S U_{ijk}^q N \,\mathrm{d}S\right]\left\{u_k^q\right\}, \tag{15}$$

in which the coefficients D_{ijk} and U_{ijk} for each q, defined below are related to the strain components which involve the derivations of H_{ij} and F_{ij}, as may be seen in Eqs. (13) and (14).

$$D_{111} = c_{11}\frac{\partial H_{11}}{\partial \xi_1} + c_{12}\frac{\partial H_{21}}{\partial \xi_2},$$

$$D_{211} = c_{11}\frac{\partial H_{12}}{\partial \xi_1} + c_{12}\frac{\partial H_{22}}{\partial \xi_2},$$

$$D_{122} = c_{12}\frac{\partial H_{11}}{\partial \xi_1} + c_{22}\frac{\partial H_{21}}{\partial \xi_2},$$

$$D_{222} = c_{12}\frac{\partial H_{12}}{\partial \xi_1} + c_{22}\frac{\partial H_{22}}{\partial \xi_2},$$

$$D_{112} = c_{66}\left[\frac{\partial H_{11}}{\partial \xi_2} + \frac{\partial H_{21}}{\partial \xi_1}\right],$$

$$D_{212} = c_{66}\left[\frac{\partial H_{12}}{\partial \xi_2} + \frac{\partial H_{22}}{\partial \xi_1}\right],$$

$$U_{111} = c_{11}\frac{\partial F_{11}}{\partial \xi_1} + c_{12}\frac{\partial F_{21}}{\partial \xi_2},$$

$$U_{211} = c_{11}\frac{\partial F_{12}}{\partial \xi_1} + c_{12}\frac{\partial F_{22}}{\partial \xi_2},$$

$$U_{122} = c_{12}\frac{\partial F_{11}}{\partial \xi_1} + c_{22}\frac{\partial F_{21}}{\partial \xi_2},$$

$$U_{222} = c_{12}\frac{\partial F_{12}}{\partial \xi_1} + c_{22}\frac{\partial F_{22}}{\partial \xi_2},$$

$$U_{112} = c_{66}\left[\frac{\partial F_{11}}{\partial \xi_2} + \frac{\partial F_{21}}{\partial \xi_1}\right],$$

$$U_{212} = c_{66}\left[\frac{\partial F_{12}}{\partial \xi_2} + \frac{\partial H_{22}}{\partial \xi_1}\right].$$

3.3. Model for numerical examples

Because of the symmetry of the geometry, material properties and loading, one half ($0 \leq y \leq W/2$) of the plate is modeled with boundary elements as shown in Fig. 2. The boundary conditions are as follows:

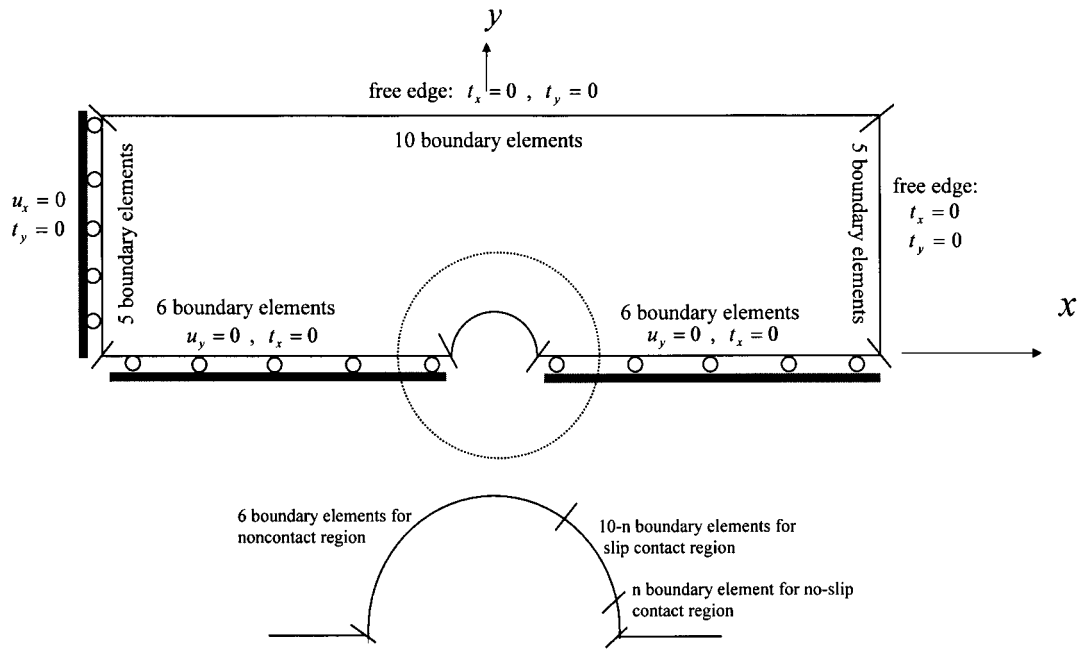

Fig. 2. Boundary element model for the pin-loaded laminates.

Along $x = -L + d_1$ (for $0 \le y \le W/2$):

$$u_x = 0 \text{ and } t_y = 0 \tag{16}$$

Along $y = 0$ (for $-L + d_1 \le x \le -R$ and $R \le x \le d_1$):

$$u_y = 0 \text{ and } t_x = 0 \tag{17}$$

Along $x = d_1$ (for $0 \le y \le W/2$) and $y = W/2$ (for $-L + d_1 \le x \le d_1$):

$$t_x = 0 \text{ and } t_y = 0 \tag{18}$$

Along the non-contact region of the hole boundary $r = R$ ($\alpha \le \phi \le 2\pi - \alpha$):

$$\sigma_r = \tau_{r\phi} = 0 \tag{19}$$

Along the contact region of the hole boundary $r = R$: follow Eqs. (3) and (4).

3.4. Computational algorithm

The computational algorithm used for determining the contact regions and stresses and displacements is outlined as follows:

Step 1. Input data including material properties, geometrical dimensions, friction coefficient μ, clearance, e, and a load, P.
Step 2. Assign values for angles α and β.

Step 3. Calculate tractions t_x, t_y and displacements u_x, u_y of nodal points on the boundary elements.
Step 4. Calculate stresses σ_r and $\tau_{r\phi}$ around the contact region of the hole according to Eqs. (5a) and (5b).
Step 5. Use the computed values of σ_r and $\tau_{r\phi}$ to check whether or not the force conditions of Eq. (4b) for β and Eq. (19) for α are satisfied.
Step 6. Repeat steps 2–5 until a converged solution is obtained.
Step 7. Calculate displacement components, u_i, and stress components, σ_{ij}, at required points, according to Eqs. (13) and (15).

4. Numerical results and discussions

In all numerical results $L = 2.5W = 254$ mm, $h = 5.08$ mm and $R = 12.7$ mm are used. For the convenience of discussion, σ and τ are used for the contact normal and shearing stresses between the pin and the hole edge, respectively. The average normal stress in the plate, $S = P/Wh$, where $Wh = 516.128\ \text{mm}^2$ and P is the total applied load in the longitudinal (x) direction from the pin.

4.1. Validity of the cosine distribution

For simplicity of analysis, the distribution of σ along a frictionless hole with zero clearance is generally assumed to vary as a cosine function of ϕ for $-\pi/2 \le \phi \le \pi/2$. The radial stress σ determined from overall equilibrium condition becomes

$$\sigma(\phi) = -\frac{4\sigma_b}{\pi}\cos\phi, \tag{20}$$

in which the average bearing stress,

$$\sigma_b = \frac{P}{Dh},$$

where D is the hole diameter and h is the total thickness of the plate. While the assumption of a cosine distribution of σ greatly simplifies the analysis, it cannot be generally valid. An orthotropic plate is examined at various levels of orthotropy to explore the validity and potential applicability of the assumption.

For an orthotropic laminate with a given set of effective longitudinal stiffness $E_{xx} = 146.757$ GPa and Poisson's ratio $\nu_{xy} = 0.26$ loaded by a perfectly fitting smooth pin at $P/h = 10$ KN/mm or $S = 0.26$ GPa, the distribution of the normal stress σ along the hole edge for various stiffness ratios of E_{xx}/E_{yy}, ranging from 1/13.481 to 13.481, are computed for three different values of $G_{xy}/E_{xx} = 0.02$, 0.1 and 0.8. They are used to examine the validity and applicability of cosine distribution assumption for σ. The derived radial stress distribution and normalized stresses along the hole boundary, for a range of stiffness ratios, are compared with the values obtained from the cosine distribution as shown in Figs. 3–5. The distribution of σ corresponding to $E_{xx}/E_{yy} = 7$, 5 and 5 agree quite well with the cosine distribution for $G_{xy}/E_{xx} = 0.02$, 0.1 and 0.8, respectively. Since the contact angle for the cosine distribution is assumed to be 90°, while the actual contact angle α is less than 90°, it may be more desirable to identify cases which closely match the cosine distribution by normalized σ and ϕ with respect to $|\sigma_0|$ and α, respectively, where $|\sigma_0|$ is the magnitude of σ at $\phi = 0$. The non-dimensionalized results presented in Figs. 3–5 indicate that $E_{xx}/E_{yy} = 13.481$, 5 and 5 give better matches. The distribution of σ deviates from the cosine distribution and may become quite severe for low values of E_{xx}/E_{yy}.

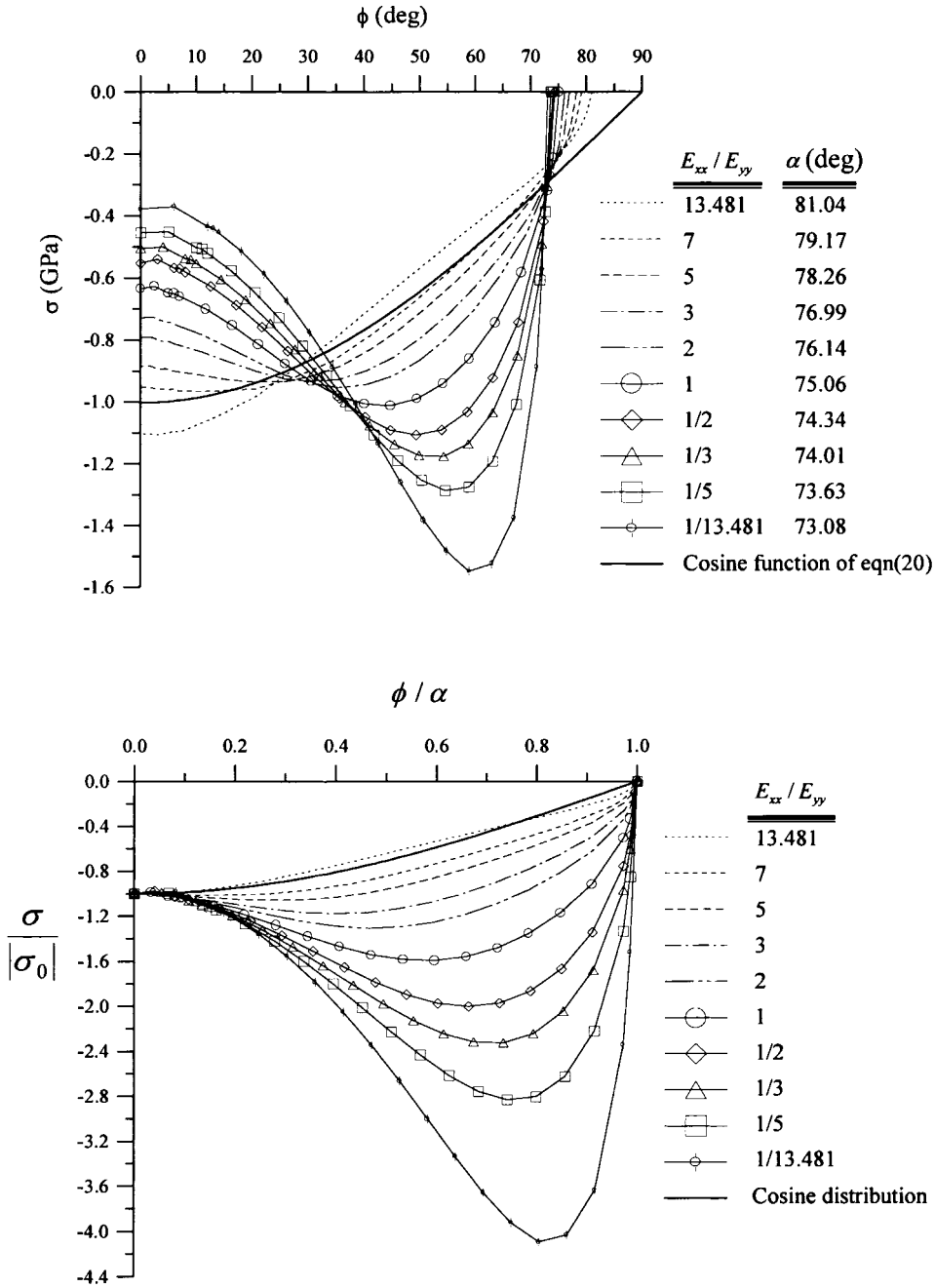

Fig. 3. Effect of stiffness ratio on σ for $E_{xx}=146.757$ GPa, $G_{xy}=0.02E_{xx}$, $\nu_{xy}=0.26$, $e=0$, $\mu=0$ and $P/h=10.0$ KN/mm ($S=0.2$ GPa).

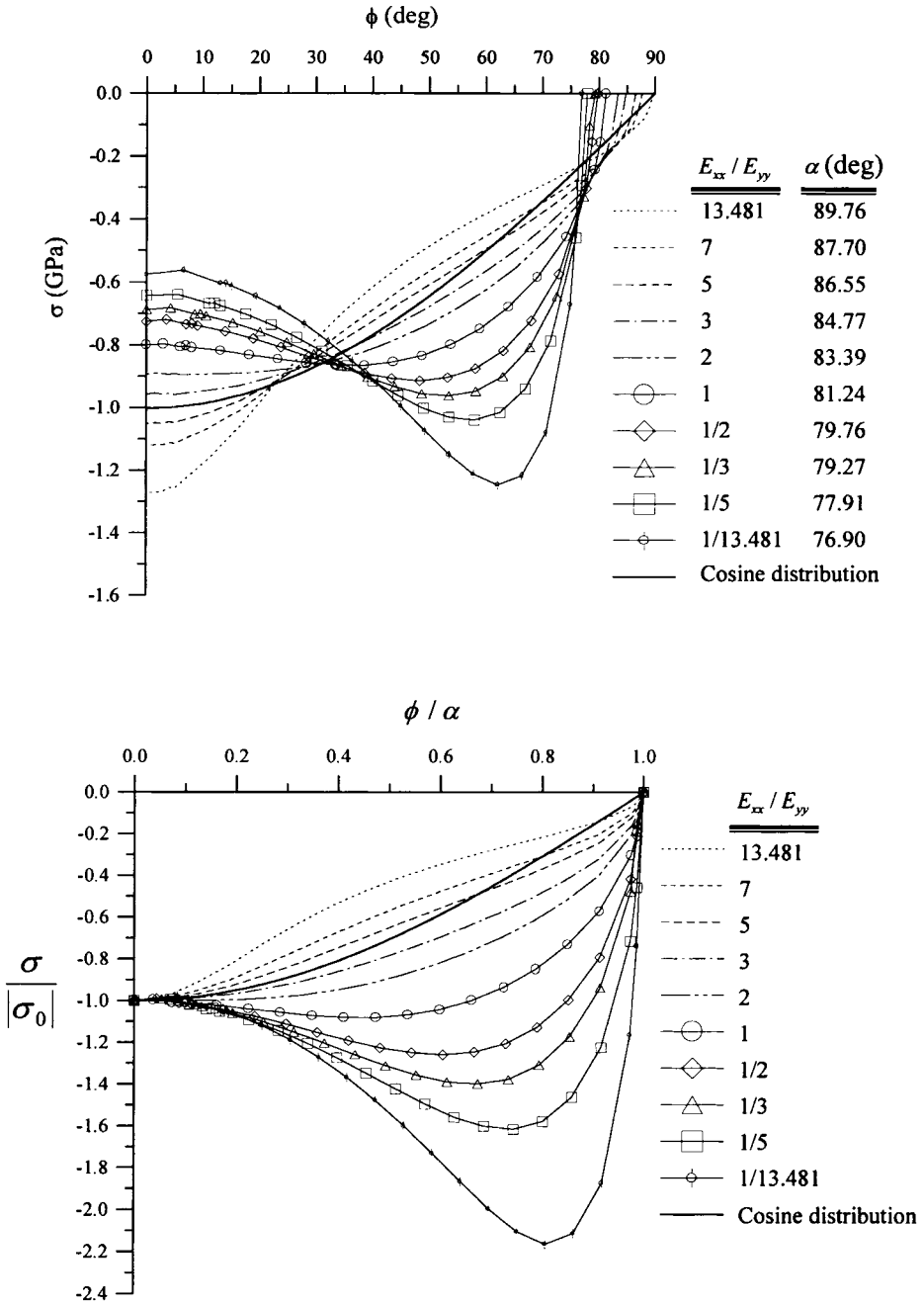

Fig. 4. Effect of stiffness ratio on σ for $E_{xx}=146.757$ GPa, $G_{xy}=0.1E_{xx}$, $\nu_{xy}=0.26$, $e=0$, $\mu=0$, and $P/h=10.0$ KN/mm ($S=0.2$ GPa).

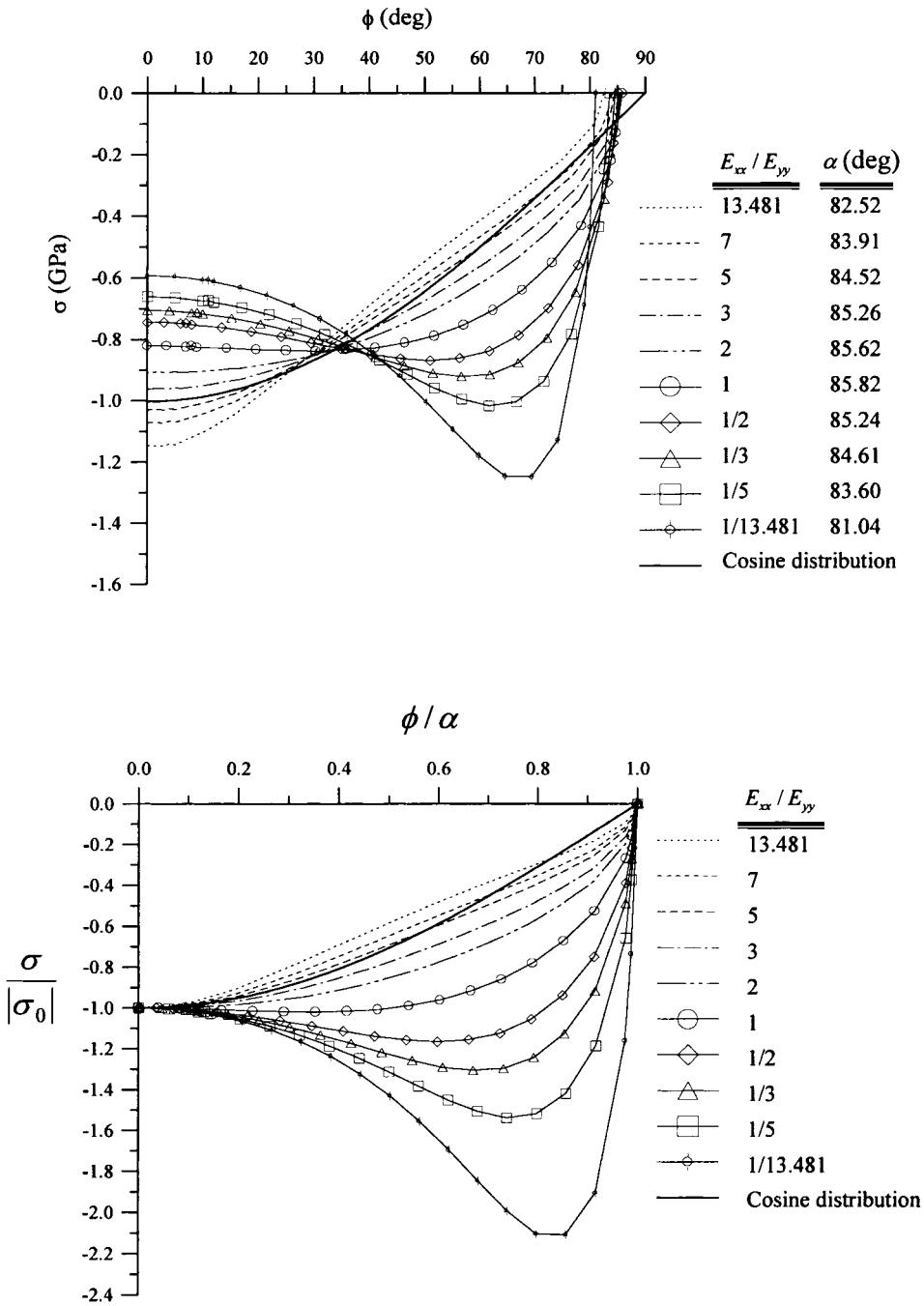

Fig. 5. Effect of stiffness ratio on σ for $E_{xx}=146.757$ GPa, $G_{xy}=0.8E_{xx}$, $\nu_{xy}=0.26$, $e=0$, $\mu=0$ and $P/h=10.0$ KN/mm ($S=0.2$ GPa).

Table 1
Mismatch Δ of displaced pin and hole edge based on cosine assumption ($\delta = 1.10$ mm, Δ for overlap if +, gap if −)

ϕ (deg)	$(x+u_x)-\delta$ (mm)	$y+u_y$ (mm)	Mismatch Δ (mm)
0	12.9688	0.0000	−0.2688
9	12.7942	1.9984	−0.2493
18	12.2750	3.9491	−0.1946
27	11.4293	5.8018	−0.1176
36	10.2850	7.5100	−0.0350
40	9.6116	8.2964	0.0030
45	8.8773	9.0311	0.0364
54	7.2470	10.3275	0.0835
63	5.4385	11.3676	0.0984
72	3.4985	12.1260	0.0794
81	1.4753	12.5850	0.0288
86	0.4477	12.6985	−0.0064
90	−0.5826	12.7338	−0.0471

Knowing that a compatible deformation of the hole edge and the pin surface cannot be maintained when the stress distribution of σ is pre-assumed, displacements at various points along the hole edge for $E_{xx}/E_{yy} = 1/13.481$ and $E_{xx} = 146.757$ GPa, $G_{xy} = 0.02E_{xx}$, $\nu_{xy} = 0.26$, $P/h = 10$ KN/mm or S = 0.26 GPa were calculated and are shown in Table 1. Values of mismatch Δ for ϕ, ranging from 0 to 90°, are also given in Table 1. The displaced pin surface and the deformed hole edge from the boundary element procedure matches very well. Since the cosine distribution of σ differs quite significantly from the actual distribution for this case as shown in Fig. 3, deformation based on the cosine assumption indicates that there are gaps and overlaps of the pin and the hole edge in the region which is assumed to be in contact. The maximum gap of 0.2443δ at $\phi = 0$ decreases as ϕ increases to about 36°, then the pin overlaps the deformed hole boundary until about 86°. The largest overlap of 0.0894δ occurs at $\phi = 63°$. The overlap Δ is defined as the distance measured from the hole edge to the pin along the radial direction with respect to the pin center O'_p after deformation. The magnitude of Δ is equal to $a - \sqrt{[(x+u_x)-\delta]^2 + (y+u_y)^2}$ and the description of Δ is shown in Fig. 6, where a negative Δ denotes the gap. It is interesting to note that while there are mismatches in the contact region when the cosine assumption is used, the deformation at the non-contact region of the hole, not in contact with the pin is in excellent agreement with the present boundary element results. A few displacements of the hole edge based on the boundary element solutions are given in Table 2 for reference.

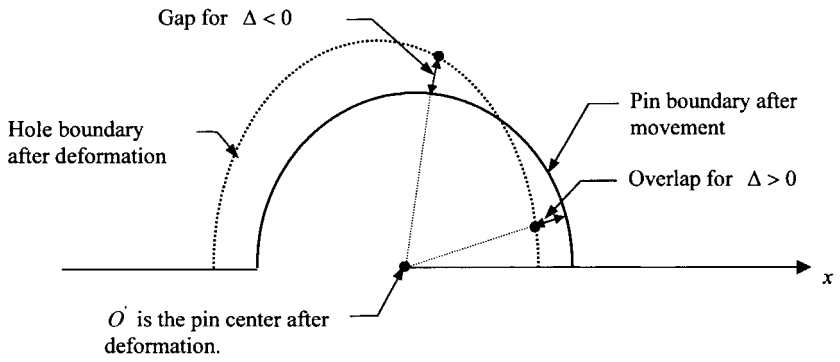

Fig. 6. The mismatch Δ between the pin and hole boundary after deformation.

Table 2
Displacements of non-contact region of the hole

ϕ (deg)	0	6	18	30	47	63	73	74	90	129	141	180
u_x (mm)	1.10	1.10	1.09	1.06	0.98	0.82	0.68	0.67	0.52	0.32	0.28	0.23
u_y (mm)	0.00	0.01	0.04	0.07	0.12	0.14	0.13	0.13	0.11	0.04	0.02	0.00

From the results to be presented later, it is found that for the case of a smooth pin without clearance, $e=\mu=0$, the contact angle α is essentially independent of the level of applied load. Hence, if the distribution of σ can be identified and represented by a cosine variation for certain laminate designs, the analysis of such pin-loaded laminates would be greatly simplified.

4.2. Effect of stiffness ratios

Data generated from investigating matters related to the cosine distribution of σ also indicate the effects of the stiffness ratios, E_{xx}/E_{yy} and G_{xy}/E_{xx}, as shown in Figs. 3–5. The three selected shear stiffness ratios of 0.02, 0.2 and 0.8 may represent low, intermediate and high values, respectively. For all three shown in Figs. 3–5, the peak normal stress σ_p occurring near $\phi=0$ for large values of the extensional stiffness ratio, decreases and gradually moves towards the edges of contact regions as E_{xx}/E_{yy} decreases. As the location of the peak normal stress moves away from $\phi=0$, the trend begins to reverse at around $\phi=25^\circ$ to 30°. The largest peak stress corresponding to the smallest E_{xx}/E_{yy} of 1/13.481 occurs at about 60° for the low and intermediate levels of shear stiffness ratio, and 70° for high G_{xy}/E_{xx} ratios.

In what follows, the contact angle, α, and the effects of e and μ are investigated for laminates with three common stacking sequences. The elasticity constants with reference to the material axes 1 and 2 are $E_{11}=146.757$ GPa, $E_{22}=10.886$ GPa, $G_{12}=6.408$ GPa and $\nu_{12}=0.38$. The effective stiffness with respect to x and y coordinates for these three laminates 1, 2 and 3 are given in Table 3. Note that angles identifying the lamination types are those between the x- and 1- coordinates. A total of 50 boundary elements with 10 of them meshed in the contact region along the hole are used.

4.3. Contact angle α

To quantitatively support the discussion made earlier on the basis of physical reasoning regarding the angle of contact, the three laminates with $\mu=0$ and $e=0$ and 0.2 mm are considered. Results for α versus applied average stress S are shown in Fig. 7. For $e=0$, α is virtually constant at 85°, 85.1° and 84.1° for laminates 1, 2 and 3, respectively, for all values of S. For $e=0.2$ mm, α increases monotonically from zero as S increases. The variation of α versus S is quite sharp for lower values of S, and becomes quite gentle for large values of S.

Table 3
Effective material properties of the laminated plates

Laminate no.	Lamination type	E_{xx} (GPa)	E_{yy} (GPa)	G_{xy} (GPa)	ν_{xy}
1	0°	146.757	10.8862	6.4077	0.38
2	$(0^\circ/\pm 45^\circ/90^\circ)$	57.85	57.85	22.077	0.31
3	90°	10.8862	146.757	6.407	0.0282

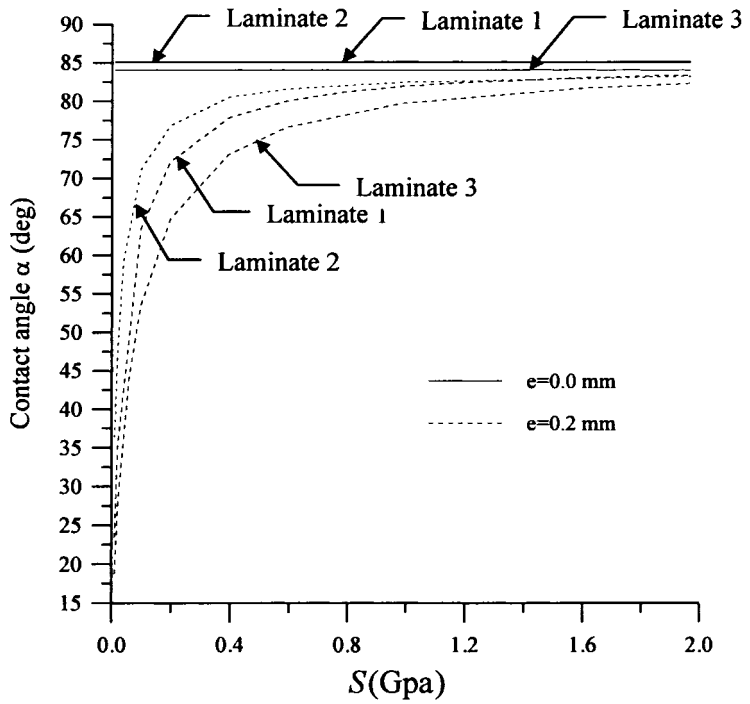

Fig. 7. Effect of pin-loaded clearance on contact angle for $\mu = 0$.

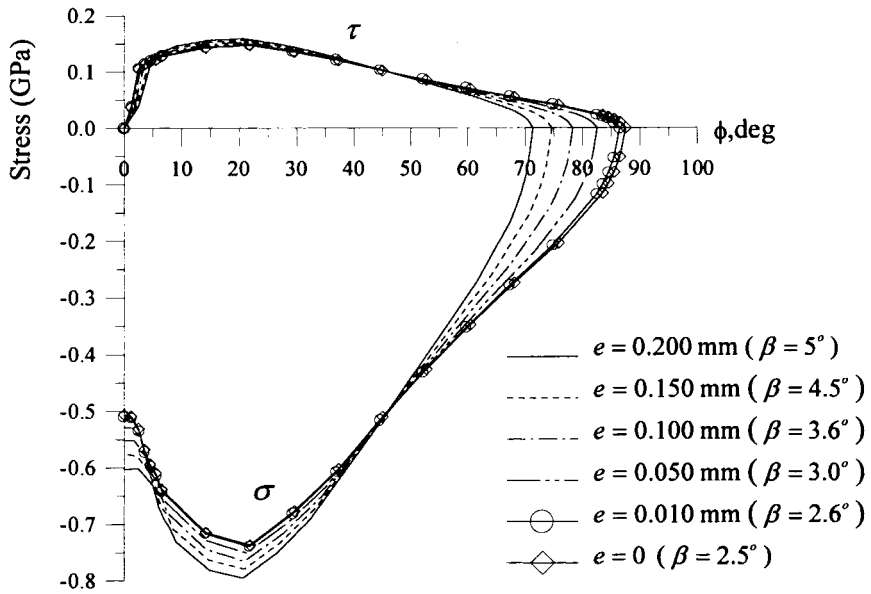

Fig. 8. Effect of pin-loaded clearance on contact stresses in Laminate 1 with $\mu = 0.2$ and $P/h = 8.1$ KN/mm ($S = 0.16$ GPa).

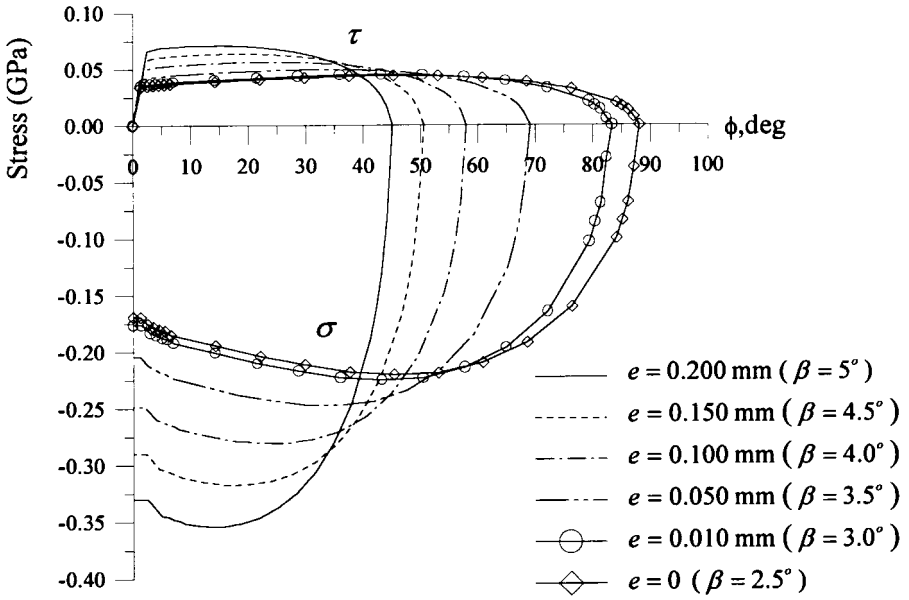

Fig. 9. Effect of pin-loaded clearance on contact stresses in Laminate 2 with $\mu = 0.2$ and $P/h = 3.0$ KN/mm ($S = 0.06$ GPa).

4.4. Effect of clearance e

Radial and shear stress distributions around the pin-loaded hole for the three laminates with $\mu = 0.2$ for $e = 0$, 0.05 mm, 0.1 mm, 0.15 mm and 0.2 mm are considered. The applied average stresses

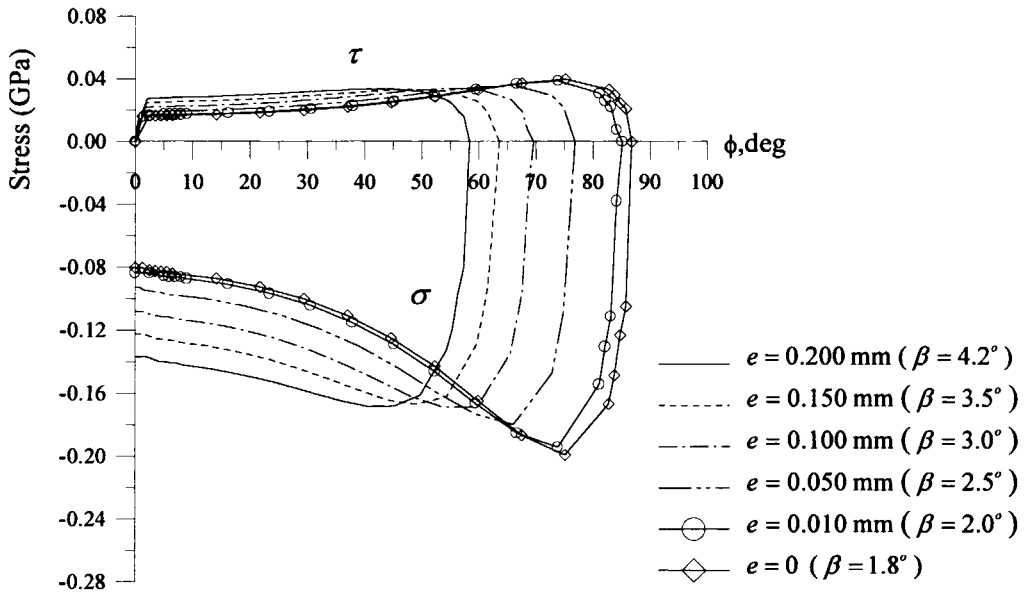

Fig. 10. Effect of pin-loaded clearance on contact stresses in Laminate 3 with $\mu = 0.2$ and $P/h = 1.8$ KN/mm ($S = 0.035$ GPa).

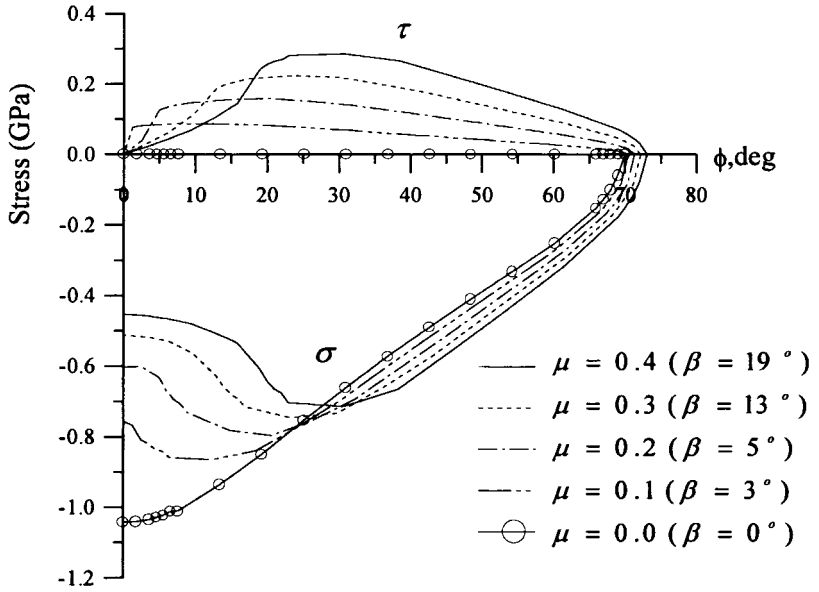

Fig. 11. Effect of pin-loaded friction on contact stresses in Laminate 1 with $e = 0.2$ mm and $P/h = 8.1$ KN/mm ($S = 0.16$ GPa).

$S = 0.16$ GPa, 0.06 GPa and 0.035 GPa for Laminates 1, 2, and 3, respectively were used. Results are shown in Figs. 8–10. The effects of e are summarized as follows:

1. The contact angle, α, decreases as e increases.
2. The peak normal stress σ_p increases as e increases for $E_{xx} > E_{yy}$ as for Laminates 1 and 2, but

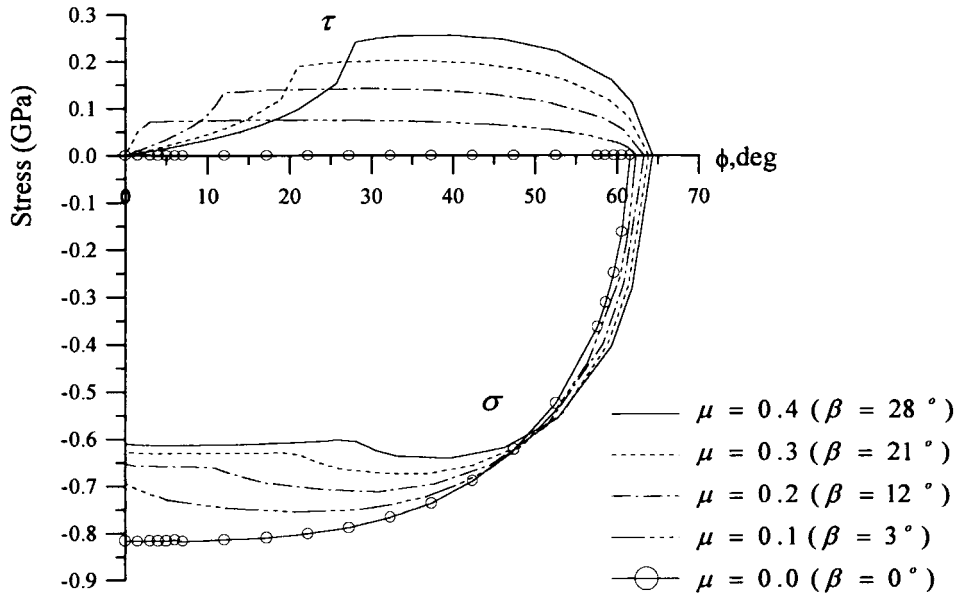

Fig. 12. Effect of pin-loaded friction on contact stresses in Laminate 2 with $e = 0.2$ mm and $P/h = 8.1$ KN/mm ($S = 0.16$ GPa).

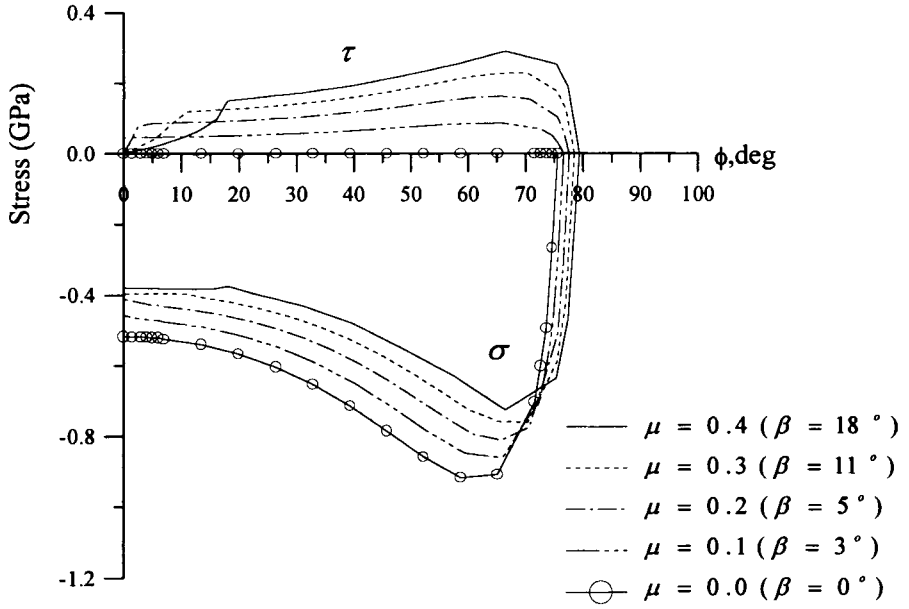

Fig. 13. Effect of pin-loaded friction on contact stresses in Laminate 3 with $e = 0.2$ mm and $P/h = 8.1$ KN/mm ($S = 0.16$ GPa).

decreases as e increases when E_{xx} becomes much less than E_{yy}, such as for Laminate 3.
3. The normal stress σ_0 at $\phi = 0$ increases as e increases.
4. The location ϕ_p of the peak normal stress clearly decreases as e increases for $E_{xx} < E_{yy}$ as Laminates 2 and 3, but is not obvious when E_{xx} becomes much larger than E_{yy} such as for Laminate 1.
5. The angle β remains a small value of less than 5° for all cases.

4.5. Effect of coefficient of friction μ

Radial and shear stress distributions around the pin-loaded hole for the three laminates with $e = 0.2$ mm under $S = 0.16$ GPa for $\mu = 0$, 0.1, 0.2, 0.3 and 0.4 are considered. Results are shown in Figs. 11–13. The effects of μ are summarized as follows:

1. The contact angle α increases as μ increases.
2. The peak normal stress σ_p decreases as μ increases.
3. The normal stress σ_0 at $\phi = 0$ decreases as μ increases.
4. The location ϕ_p of the peak normal stress increases as μ increases.
5. The angle β increases as μ increases.

5. Empirical formulae

A number of analytical and numerical methods discussed in the introduction are available for analyzing plates with a pin-loaded hole, provided the stresses along the hole boundary are given. The cosine distribution of contact normal stress was generally assumed in the past. However, in order to

prescribe a correct traction distribution along the hole boundary, the interaction of the pin and plate must be considered first, which is the difficult part. While the boundary element method developed in the study has shown its capability of determining the interacting stresses along the hole boundary, the process requires a fair amount of knowledge in the boundary element method with considerable familiarity and experience in the computer program. As a result, this represents some what of a hurdle or tedium in the entire analysis process of the pin-loaded plate problems for designers. To help reduce the effort of specifying more realistic tractions distribution along the hole boundary, empirical formulae based on data generated by the present boundary element method would be useful to users having their own follow-up programs, including the present one for determining stresses and deformation of the plate; it also may help simplify the design process when repeated calculations for determining stresses and deformation are needed. By reviewing a large quantity of numerical results, common trends of stress distribution along the hole boundary are noted. Therefore, it appears possible that empirical formulae for contact stresses between the pin and the hole boundary may be established. The process and procedure for establishing the empirical formulae for a representative case is presented for illustrative purposes, and a limited database has been generated for this one class of problems which is believed to be realistic. The commonly used graphite epoxy as the basic lamination material, and widely used stacking sequence classified as Laminates 1, 2, and 3 before are considered here. Their effective material properties are given in Table 3. Numerical results such as those presented in Figs. 8–13 for the configuration considered in this study exhibit common trends of stress variation along the hole boundary for various clearances and coefficients of friction. It appears adequate to represent an empirical equation in two segments for the contact normal pressure, and each segment may be represented by a polynomial in non-dimensional form such as

$$\bar{\sigma} = \bar{\sigma}_0[1 - 2\eta^2 + \eta^4] + 2\eta^2 - \eta^4 \text{ for } 0 \le \eta \le 1 \tag{21}$$

and

$$\bar{\sigma} = 1 - \left(\frac{\zeta - \zeta_p}{1 - \zeta_p}\right)^2 + \Theta(\zeta - \zeta_p)^2\left[(\zeta - \zeta_p)^{m-2} - (1 - \zeta_p)^{m-2}\right] \text{ for } \zeta_p \le \zeta \le 1, \tag{22}$$

for $m > 2$, where $\eta = \phi/\phi_p$, $\zeta = \phi/\alpha$, and $\bar{\sigma} = \sigma/\sigma_p$. The subscripts '0' and 'p' denote the locations of the associated quantities at $\phi = 0$ and the point having the peak contact normal stress, respectively. The suggested formulae given in Eqs. (21) and (22) satisfy the following conditions:

$$\sigma = \sigma_0 \text{ and } \frac{d\sigma}{d\phi} = 0 \text{ at } \phi = 0,$$

$$\sigma = \sigma_p \text{ and } \frac{d\sigma}{d\phi} = 0 \text{ at } \phi = \phi_p$$

and

$$\sigma = 0 \text{ at } \phi = \alpha.$$

The power m is left to be selected to give a desirable fit to the σ–ϕ curves, and the simplest case is to take $m = 3$. The constant Θ is to be determined by satisfying the equipollence of the resultant of contact stresses and the applied load, resulting in the following condition:

$$P = \int_0^{\alpha} -\sigma \cos\phi R \, d\phi + \int_0^{\alpha} \tau \sin\phi R \, d\phi$$

$$= \int_0^{\alpha} -\sigma \cos\phi R \, d\phi + \int_0^{\beta} \tau \sin\phi R \, d\phi + \int_{\beta}^{\alpha} \mu(-\sigma)\sin\phi R \, d\phi, \tag{23}$$

which involves the following integrals

$$S_n = \int \phi^n \sin\phi \, d\phi \quad \text{and} \quad C_n = \int \phi^n \cos\phi \, d\phi,$$

where $S_0 = -\cos\phi$, $C_0 = \sin\phi$, $S_n = nC_{n-1} - \phi^n \cos\phi$ and $C_n = -nS_{n-1} + \phi^n \sin\phi$. Empirical Eqs. (21) and (22) accurately represent the results presented in Fig. 8, where ϕ_p is much smaller than α. If the region from $\phi = 0$ to ϕ_p occupies a large portion of the entire contact region such as those presented in Fig. 10, the last term in Eq. (22) may be omitted and a similar term be added in Eq. (21). It should be noted here that Eqs. (21) and (22) are probably the simplest form suggested for the geometry and loading of the laminates considered in this study. They may be further improved by adding higher order terms if desired.

The shear stress $\tau = \mu\sigma$ for the slip region, and varies from 0 to $\mu\sigma_\beta$ for $\phi = 0$ to β for the no-slip region where σ_β is the normal contact stress at $\phi = \beta$. The shear stress distribution in the no-slip region may be represented by a unit step function with a magnitude of $\mu\sigma_\beta$ for cases having a small β, and a linear or quadratic functions for ϕ varying from 0 to $\mu\sigma_\beta$ for larger values of β. The linear variation is used in this study. At any rate, it may be noted here that one only needs to establish empirical formulae for contact normal stress. As mentioned before, Figs. 8–13 contains two classes of results. Class 1 are those associated with results such as those in Figs. 8–10 and correspond to the variation of clearances, and Class 2 are those associated with Figs. 11–13 and correspond to the variation of the coefficient of friction. Interpolation functions for classes 1 and 2 may be represented by linear functions of e and quadratic functions of μ, respectively as follows:

Class 1:

$$\lambda = \lambda_l - \frac{\lambda_l - \lambda_s}{e_l - e_s}(e_l - e) \tag{24}$$

Class 2:

$$\lambda = \lambda_s + \frac{1}{\mu_l \mu_m (\mu_l - \mu_m)} \left\{ \left[\mu_l^2 \lambda_m - \mu_m^2 \lambda_l + \left(\mu_m^2 - \mu_l^2 \right) \lambda_s \right] \mu + \left[\mu_m \lambda_l - \mu_l \lambda_m + (\mu_l - \mu_m) \lambda_s \right] \mu^2 \right\}, \tag{25}$$

where λ stands for β, α, ϕ_p, σ_0, σ_β and σ_p, whichever parameter is under consideration. Data similar to the results shown in Fig. 7 for β, α, ϕ_p, σ_0, σ_β and σ_p corresponding to e_s, e_l, μ_s, μ_m and μ_l under a range of S have been generated to establish the database. For illustrative purposes, results presented in Figs. 8 and 11 for the plate under $P/h = 8.1$ KN/mm or S = 0.16 GPa are revisited. The values of β, α, ϕ_p, σ_0, σ_β and σ_p corresponding to e_s and e_l are given in Table 4 for $\mu = 0.2$ for all three laminates. Their values corresponding to μ_s, μ_m and μ_l for $e = 0.2$ mm are given in Table 5.

As a first numerical example, we consider $\mu = 0.2$ and $e = 0.1$ mm. Using the interpolation equation Eq. (24), the values of β, α, ϕ_p, σ_0, σ_β and σ_p are found to agree well with the results obtained directly from the boundary element program. The overall variation of contact normal stress σ using several test values of m in the empirical formulae are all compared reasonably well with the boundary element solutions as shown in Fig. 14. It is judged that $m = 3$ gives the best approximation for this case, and is

Table 4
Key quantities for empirical formula ($\mu = 0.2$)

Laminate no.		e	σ_0	σ_p	σ_β	ϕ_p (deg)	α (deg)	β (deg)
1	e_l	0.2	−0.6029	−0.7952	−0.6313	20.7	71.5	5.0
	e_s	0.0	−0.5058	−0.7372	−0.5300	21.9	87.6	2.5
2	e_l	0.2	−0.3123	−0.3547	−0.3452	15.4	45.2	5.0
	e_s	0.0	−0.1692	−0.2204	0.1753	45.3	88.1	2.5
3	e_l	0.2	−0.1338	−0.1683	0.1397	40.6	58.5	4.2
	e_s	0.0	−0.0804	−0.1992	0.0820	75.2	86.8	1.8

also true for the $e = 0$ and 0.2 mm cases, although detailed results are omitted here. The maximum deviation of σ based on the empirical formulae is roughly estimated to be less than 9 percent below the boundary element solution at $\phi = 10^\circ$, where $\phi_p = 21.3^\circ$. To examine the contact normal stress distribution corresponding to the key quantities given in Table 5 which are used in the interpolation equation Eq. (25), results based on the empirical formulae for various value of m all compare reasonably well with the boundary element solutions except those near the end for values of ϕ close to α where low normal stresses occur as shown in Figs. 15 and 16. Again, $m = 3$ is judged to give the best representation. As a second numerical example, we judge that $\mu = 0.1$, $e = 0.2$ mm, and $m = 3$ give the best approximation. Through the interpolation equation Eq. (25), results are presented in Fig. 17. The key parameters as well as the normal stress distribution along the contact region agree well with the boundary element solutions except for the normal stresses near $\phi = \alpha$ having low values. The empirical results for the peak stress σ_p and the normal stress σ_0 at $\phi = 0$ are about 3.4 and 3.8 percent higher than the boundary element results, respectively.

6. An example

Results of one of the case for laminate 1 with $\mu = 0.2$ and $e = 0$ presented earlier are used here to help summarize the analysis procedure. These results are contained in Figs. 7 and 8, and Table 4. The contact angle, α, for a range of loading is shown in Fig. 7 which is a representative figure in the database for λ denoting β, α, ϕ_p, σ_0, σ_β and σ_p. From Fig. 7 and as discussed before, since $e = 0$, one may consider α, β and ϕ_p to be independent of loading. Their values are given in Table 4 as 87.56°, 2.5° and 21.9°, respectively. As a result, stresses and deformation become linear functions of the applied far

Table 5
Key quantities for empirical formula ($e = 0.2$ mm)

Laminate no.		μ	σ_0	σ_p	σ_β	ϕ_p (deg)	α (deg)	β (deg)
1	μ_l	0.4	−0.4532	−0.7136	−0.6077	30.7	73.0	19.0
	μ_m	0.2	−0.6036	−0.7957	−0.6319	20.7	71.3	5.0
	μ_s	0.0	−1.0422	−1.0422	0.0	0.0	70.0	0.0
2	μ_l	0.4	−0.6102	−0.6410	−0.6050	39.6	64.3	28.0
	μ_m	0.2	−0.6532	−0.7121	−0.66897	30.8	63.3	12.0
	μ_s	0.0	−0.8161	−0.8174	0.0	7.0	61.6	0.0
3	μ_l	0.4	−0.3796	−0.7254	−0.3744	66.5	79.4	18.0
	μ_m	0.2	−0.41145	−0.8105	−0.4284	65.8	77.6	5.0
	μ_s	0.0	−0.5183	−0.9172	0.0	58.7	75.7	0.0

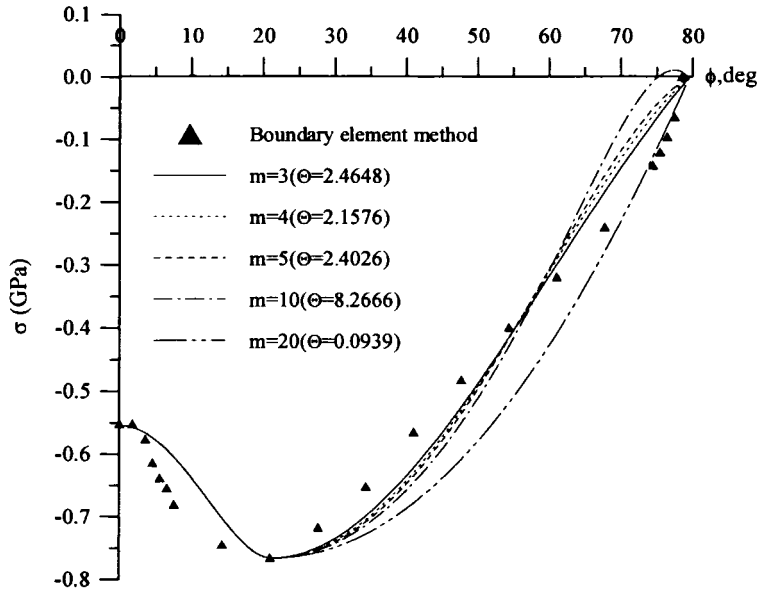

Fig. 14. Effect of the power m of empirical formulae on contact stresses for Laminate 1 with $e = 0.1$ mm, $\mu = 0.2$, $P/h = 8.1$ KN/mm ($S = 0.16$ GPa).

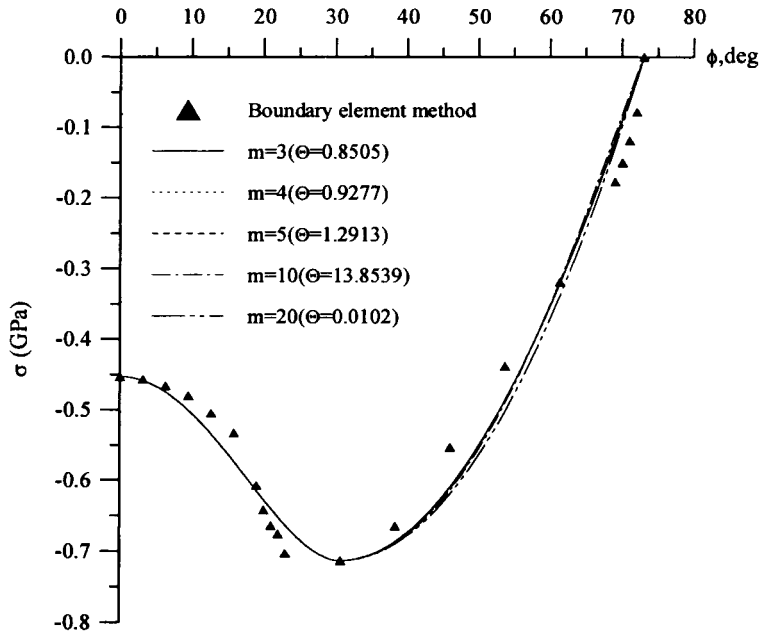

Fig. 15. Effect of the power m of empirical formulae on contact stresses for Laminate 1 with $e = 0.2$ mm, $\mu = 0.4$, $P/h = 8.1$ KN/mm ($S = 0.16$ GPa).

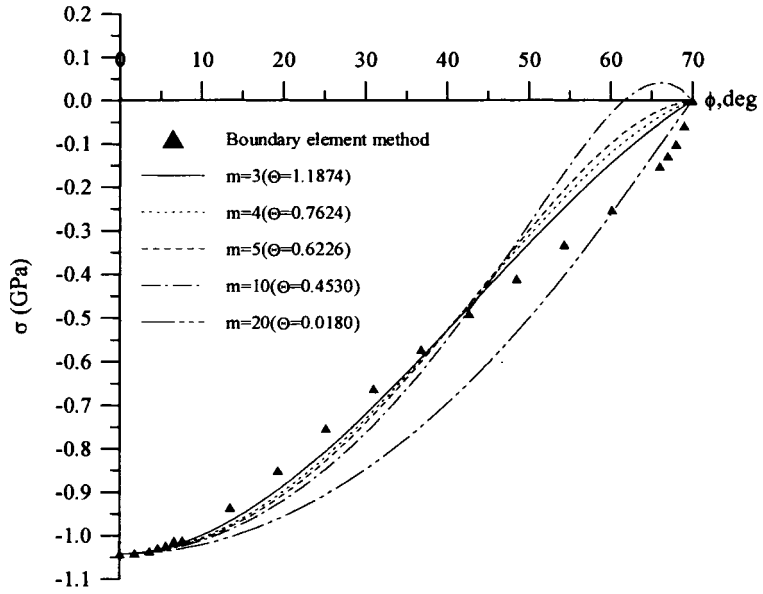

Fig. 16. Effect of the power m of empirical formulae on contact stresses for Laminate 1 with $e = 0.2$ mm, $\mu = 0$, $P/h = 8.1$ KN/mm ($S = 0.16$ GPa).

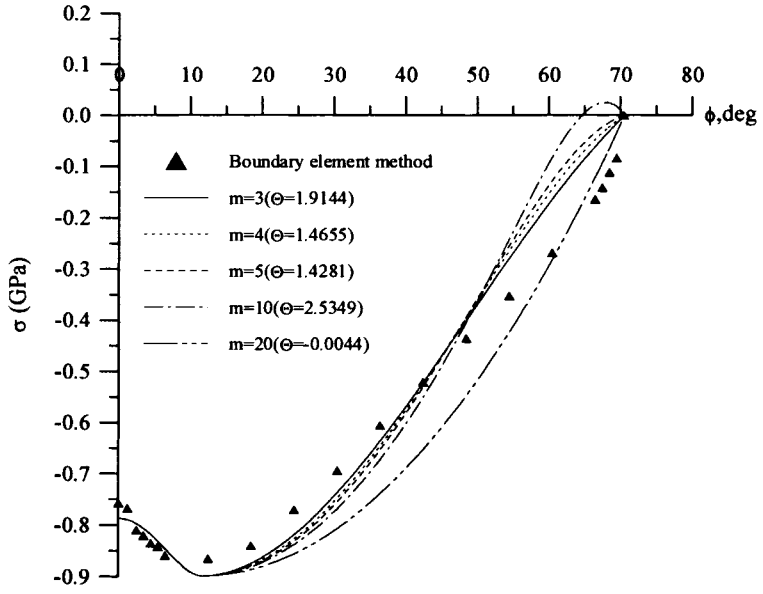

Fig. 17. Effect of the power m of empirical formulae on contact stresses for Laminate 1 with $e = 0.2$ mm, $\mu = 0.1$, $P/h = 8.1$ KN/mm ($S = 0.16$ GPa).

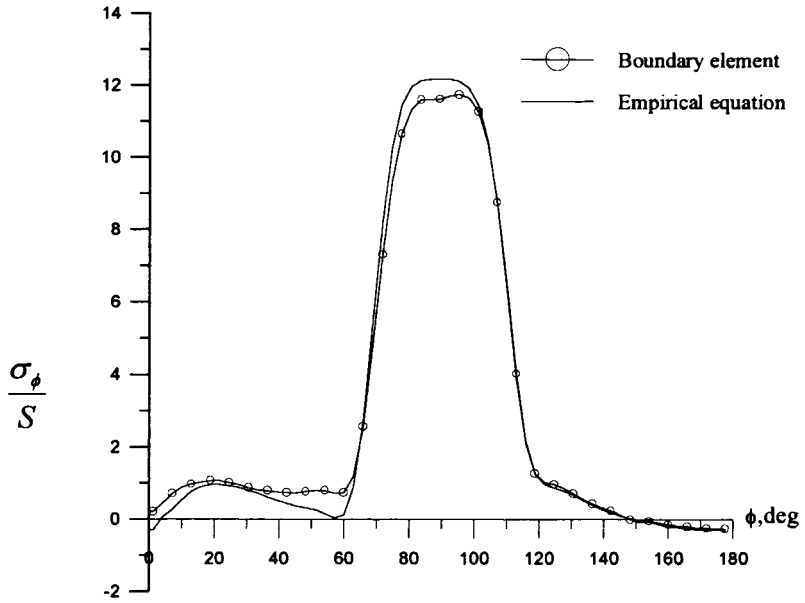

Fig. 18. Circumferential stress along hole-edge for Laminate 1 with $e = 0$, $\mu = 0.2$.

field stress S. The contact normal and shear stress distributions for this case are shown in Fig. 8 for $S = 0.16$ GPa. Based on the data given in Fig. 8, one may continue to use the present boundary element program to calculate stresses and displacement at any point of the plate. On the other hand, one may use the empirical formulae in conjunction with the interpolation equations to specify tractions along the hole boundary and follow up with any other existing stress analysis programs, including the present one as mentioned before. When the present boundary element program is used for the direct calculation as well as through the empirical procedure, the contact normal and shear stresses agree well with each other, a topic which has been discussed earlier. Results on the circumferential stress, σ_ϕ, along the hole edge based on the empirical procedure also agree well with those using the present boundary element method directly; these are shown in Fig. 18.

7. Conclusions

Several aspects concerning the validity and applicability of cosine distribution of contact normal stress, effects of stiffness ratio as well as clearance and friction are addressed and investigated through numerical results.

The direct boundary element procedure developed by Lin and Lin (1999) has been refined, improved and extended. The procedure provides high computational efficiency which allows one to generate sufficient amount of data for the possibility of establishing empirical formulas to facilitate design applications. It also has the capability of determining stresses and displacements at points on the boundaries as well as in the interior part of laminates. On the basis of the numerical results, the following conclusions may be made:

1. While the assumption of cosine distribution of contact normal stress greatly simplifies the analysis procedure, it may only be applicable to laminates having very specific extensional stiffness ratios as

indicated in Figs. 3–5. The cosine distribution is different from the actual distribution in general, and the discrepancy could become quite significant.
2. The shear stiffness ratio G_{xy}/E_{xx} does not seem to have a significant effect on the general trend of contact stresses for all extensional stiffness ratios, E_{xx}/E_{yy}, considered.
3. The contact angle, α, essentially remains constant for the case of zero clearance. For $e > 0$, α increases sharply as S increases at lower values of S, and the rate of increase becomes quite mild for large values of S.
4. The contact angle, α, decreases as e increases, and the peak normal stress, σ_p, increases as e increases for $E_{xx} > E_{yy}$ as for Laminates 1 and 2, but decreases as e increases when E_{xx} becomes much less than E_{yy}, such as for Laminate 3.
5. The contact angle, α, increases as μ increases, and the peak normal stress, σ_p, decreases as μ increases.
6. The simple forms of the empirical formulae suggested in the study appear to work well for the examples presented. In place of the cosine assumption of contact normal stress distribution, the empirical formulae for contact normal and shear stresses give more reliable results and help simplify the analysis of pin-loaded laminates.

Acknowledgements

The study was supported by the National Science Council of the Republic of China (TAIWAN) under Grant NSC 88-2212-E-005-001.

References

Agarwal, B.L., 1980. Static strength prediction of bolted joint in composite material. AIAA Journal 18 (11), 1371–1375.

Banerjee, P.K., Butterfield, R., 1981. Boundary Element Method in Engineering Science. McGraw–Hill, Maidenhead, UK.

Blackie, A.P., Chutima, S., 1996. Stress distributions in multi-fastened composite plates. Composite Structures 34, 427–436.

Camanho, P.P., Mattews, F.L., 1997. Stress analysis and strength prediction of mechanically fastened joint in FRP: A review. Composites — Part A: Applied Science and Manufacturing 28 (6), 529–547.

Chang, F.K., Scott, R.A., Springer, G.S., 1983. Strength of mechanically fastened composite joints. Journal of Composite Materials 16, 470–494.

Chang, F.K., Scott, R.A., 1984a. Failure of composite laminates containing pin loaded holes — method of solution. Journal of Composite Materials 18, 255–278.

Chang, F.K., Scott, R.A., 1984b. Failure strength of nonlinearly elastic composite laminates containing a pin loaded hole. Journal of Composite Materials 18, 464–477.

Chang, F.K., 1986. The effect of pin load distribution on the strength of pin loaded holes in laminated composites. Journal of Composite Materials 20, 401–408.

Cooper, C., Turvey, G.J., 1995. Effects of joint geometry and bolt torque on the structural performance of single bolt tension joints in pultruded GRP sheet material. Composite Structures 32, 217–226.

Eriksson, I., Backlund, J., Moller, P., 1995. Design of multiple-row bolted composite joints under general in-plane loading. Composite engineering joints and adhesion. In: Proceedings of the International Conference for Composite Engineering, vol. 5, issue 8, pp. 1051–1068.

Eshwar, V.A., 1978. Analysis of clearance fit pin joints. International Journal of Mech. Sci. 20, 485–491.

Ghosh, B.D., Rao, A.K., 1981. Load transfer from a smooth elastic pin to a large sheet. AIAA Journal 18 (5), 619–625.

Hyer, M.W., Klang, E.C., 1985. Contact stresses in pin-loaded orthotropic plates. International Journal of Solids and Structures 21 (9), 957–975.

Hyer, M.W., Klang, D.C., Cooper, D.E., 1987. The effects of pin elasticity, clearance, and friction on the stresses in a pin-loaded orthotropic plate. Journal of Composite Materials 21, 190–206.

Jong, T.D., 1977. Stresses around pin-loaded holes in elastically orthotropic or isotropic plates. Journal of Composite Materials 11, 313–331.

Lin, C.C., Lin, C.H., 1993. Stress and strength analysis of bolted composite joints using direct boundary element method. Journal of Composite Structures 25, 209–215.

Lin, C.C., Lin, C.H., 1999. Stresses around pin-loaded hole in composite laminates using direct boundary element method. International Journal of Solids and Structures 25, 209–215.

Lin, C.H., 1998. Analysis of Pin-Loaded Plates by a Boundary Element Method. Ph.D. dissertation, National Chung-Hsing University, Taichung, Taiwan.

Mahajerin, E., Sikarskin, D.L., 1986. Boundary element study of a loaded hole in an orthotropic plate. Journal of Composite Materials 20, 375–389.

Mangalgiri, P.D., Ramamurthy, T.S., Dattaguru, B., Rao, A.K., 1987. Elastic analysis of pin joints in plates under some combined pin and plate loads. International Journal Mech. Sci. 29 (8), 577–585.

Naik, R.A., Crews, J.H., 1986. Stress analysis method for a clearance-fit bolt. AIAA Journal 24 (8), 1348–1353.

Quinn, W.J., Matthews, F.L., 1977. The effect of stacking sequence on the pin-bearing strength in glass fibre reinforced plastic. Journal of Composite Materials 11, 139–145.

Pyner, G.R., Matthews, F.L., 1979. Comparison of single and multi-hole bolted joints in glass fibre reinforced plastic. Journal of Composite Materials 13, 232–239.

Rahman, M.U., 1984. An iterative procedure for finite-element stress analysis of frictional contact problems. Computers & Structures 18 (6), 947–954.

Rahman, M.U., Rowlands, R.E., 1993. Finite element analysis of multiple bolted joints in orthotropic plates. Computers & Structures 46 (5), 859–867.

Rizzo, F.J., Shippy, D.J., 1970. A method for stress determination in plane anisotropic elastic bodies. Journal of Composite Materials 4, 36–61.

Tsai, M.Y., Morton, J., 1990. Stress and failure analysis of pin-loaded composite plate: An experimental study. Journal of Composite Materials 24, 1101–1121.

Tsujimoto, Y., Wilson, D., 1986. Elasto–plastic failure analysis of composite bolted joints. Journal of Composite Materials 20, 236–252.

Waszczak, J.P., Cruse, T.A., 1971. Failure mode and strength predictions of anisotropic bolt bearing specimens. Journal of Composite materials 5, 421–425.

Wong, S., Matthews, F.L., 1981. A finite element analysis of single and two-hole bolted joints in fibre reinforced elastic. Journal of Composite Materials 15, 481–491.

Yogeswaren, E.K., Reddy, J.N., 1988. A study of contact stresses in pin-loaded orthotropic plates. Computers & Structures 30 (5), 1067–1077.

Zhang, K.D., Ueng, C.E.S., 1984. Stresses around a pin-loaded hole in orthotropic plates. Journal of Composite Materials 18, 432–446.